1 **Microwave-assisted preparation of almond shell-based activated carbon for**

2 **methylene blue adsorption**

3 Chunfeng Du[a], Hongbing Yang[a], Zhansheng Wu [a, b*], Xinyu Ge[a], Giancarlo Cravotto[b],

4 Bang-Ce Ye[a], Imdad Kaleem[c]

5 a School of Chemistry and Chemical Engineering, Shihezi University, Shihezi 832003, P.R.

6 China

7 b Dipartimento di Scienza e Tecnologia del Farmaco, University of Turin, Turin 10125, Italy

8 c COMSATS Institute of Information Technology (CIIT), Islamabad, 45550, Pakistan.

9 Corresponding author: Zhansheng Wu, Shihezi University, Shihezi 832003, P.R. China.

10 Tel: 86993-2055015, Fax: 86993-2057270. E-mail address: wuzhans@126.com

11

Abstract

In this study, a novel adsorbent designated as almond shell-based activated carbon (ASAC) was synthesized from waste almond shells (AS) through exposure to microwave radiations and usage of $ZnCl_2$ as a chemical activator. The ramifications of synthetic conditions were further elaborated by response surface methodology to optimize the adsorption capacity of ASAC for methylene blue (MB) dye. The determined optimized conditions of ASAC preparation were such as: mass ($ZnCl_2$/AS) ratio of 3:1 (w/w) and microwave heating time period of 15 min at 900 W, while the maximum obtained yield of ASAC was 39.67%, with an adsorption capacity of 314.20 mg/g for MB. In addition, ASAC was characterized by N_2 adsorption-desorption measurement, scanning electron microscopy, Fourier-transform infrared spectrometry (FTIR), X-ray photoelectron spectroscopy (XPS) and point of zero charge measurement. The optimized ASAC had a Brunauer-Emmett-Teller surface area of 839.60 m^2/g and a total volume of 0.406 cm^3/g. FTIR and XPS analysis exhibited a decline in oxygen-containing groups of ASAC as compared with AS. The adsorption behavior of ASAC for MB was fitted well to the pseudo-second-order model and the Langmuir isotherm model. These findings support the economical and promising preparation of ASAC to be employed in environmental remediation.

Keywords: Activated carbon; Microwave; Almond shell; Response surface methodology; Methylene blue.

1. Introduction

In recent years, activated carbon (AC) has been widely employed in chemical industry due to its textural characteristics, high surface area, and surface adsorption properties. It has a very broad range of industrial applications such as separation/purification of liquids and gases, removal of toxic substances, catalysts and catalyst support, super capacitors, electrodes and gas storage [1]. One of the biggest challenges in commercial manufacturing of AC is to find a novel inexpensive precursor that has potential economic benefits and is available in large quantities to meet its rising demands. So far, many efforts have been made to produce AC from renewable sources and precursors from agricultural wastes such as oil palm shell [2], coconut husk [3], rambutan peel [4], edible fungi residues [5], and acorn shell [6]. Xinjiang, the largest autonomous region of China, produces a large amount of almond shells (AS) annually, and its annual output reached up to 60,000 tons in 2014 making it a significantly important agricultural waste. The utilization of such waste material like AS in the commercial production of AC would facilitate the development of a low-cost alternative precursor.

Due to heavy industrialization, there is a continuous emission of various pollutants in the environment particularly dyes which cause a serious threat to aquatic life. Methylene blue (MB) is the most commonly used substance in the dying process and has potential risks towards the environmental pollution; therefore, it was selected as a model adsorbate in this study to determine the adsorption efficiency of our novel synthetic adsorbent.

The general process of AC production requires high heat energy which is provided by two different ways such as conventional heating and microwave heating [7]. Conventional heating method is usually used in the industrial preparation of AC which demands higher activation

3

55 temperature and longer activation time, thereby leading to considerably lower yield and

56 higher energy cost. Achawa et al. prepared the coconut shell-based activated carbon by

57 conventional heating method by physical activation for 120 min, the result material had a

58 surface area (S_{BET}) of only 524 m^2/g [8]. Microwaves supply energy to the carbon particles,

59 and this energy is converted into heat within the particles themselves by dipole rotation and

60 ionic conduction [9]. Microwave heating has been recently employed for the preparation of

61 AC. Junior et al. synthesized a highly porous AC from macadamia nut endocarp by chemical

62 activation with $ZnCl_2$ via microwave radiations [10]. Njoku et al. also introduced a

63 microwave-induced activation process to prepare a high-surface area AC from rambutan peel

64 [4]. Hesas et al. revealed AC production from oil palm shells through microwave-induced

65 $ZnCl_2$ activation [2]. By using microwave technique, it is possible to produce activated carbon

66 by an easy and a quick way, it has potential benefits over conventional heating such as short

67 treatment time, low energy cost, high heating rate, selective heating, and controllable heating

68 process [11, 12]. All recent reports have validated the use of microwave-induced activation

69 process due to its faster activation rate and higher carbon yield. Therefore, microwave heating

70 is considered as a viable alternative for conventional heating methods.

71 Response surface methodology (RSM) has a great significance in the optimization of the

72 process conditions, analyzing the interaction between the effective process parameters, and

73 identification of the factor settings that optimize the response [3]. The RSM method has been

74 employed by many researchers to amplify AC production by using conventional heating

75 methods [13]. Hence, RSM has sound applications in refined and optimized production of

76 ACs. However, to the best of our knowledge, not a single research work is available on RSM

77 based optimized synthetic conditions for AS-derived ASAC production via microwave

78 heating.

79   The present study designed to investigate the use of microwave-induced activation

80 procedure to prepare highly porous almond shell-based activated carbon from AS, and its

81 adsorption efficiency for MB. The influences of activation time, microwave power, and mass

82 ratio on MB adsorption and yield of ASAC were thoroughly investigated. We used

83 Box–Behnken design (BBD) to select the effects of the three main variables and RSM to

84 optimize the synthetic conditions. In addition, scanning electron microscopy (SEM),

85 Fourier-transform infrared spectrometry (FTIR), X-ray photoelectron spectroscopy (XPS),

86 and other analytical techniques were used to characterize ASAC. Furthermore, the adsorption

87 isotherms and kinetics were also elucidated. The proposed synthetic method of ASAC through

88 microwave heating has a great potential in economical production of an excellent adsorbent

89 having an enormous remedial effects against various industrial wastes particularly for water

90 pollutants.

91 ## 2. Materials and methods

92 ### 2.1 Raw material

93   The AS was purchased from the local market, washed with distilled water and dried in an

94 oven at 100 °C for 24 h to remove the moisture content. The dried AS were crushed and

95 sieved to a uniform particle size of 100 meshes. The proximate analyses of AS were ash

96 1.67%, fixed carbon 29.40%, moisture 5.31% and volatilizes 63.62%. All analyses were

97 performed in three replicates.

98 ### 2.2 Preparation of ASAC

99   The microwave-assisted process was performed using a modified microwave oven

100 (MM823LA6-NS, Midea) at a frequency of 2.45 GHz. The 4.0 g of mixture with different

101 mass ratios (X_1) of $ZnCl_2$ and AS of a particle size of 100 meshes were put in a quartz tube

102 reactor placed into microwave oven. Then the activation processes were subjected to different

103 microwave heating times (X_2, min) and microwave radiation powers (X_3, W) under 100

104 cm^3/min of nitrogen flow. The resulting material was washed repeatedly with hot distilled

105 water until the pH solution reached a value of 7.0. The obtained ASAC were dried at 80 °C

106 for 24 h, and then stored for further analyses.

107   The percentage of ASAC yield was calculated using the following equation:

108 $$Y\ (\%) = \frac{W}{W_0} \times 100 \tag{1}$$

109 where W is the weight of the prepared ASAC after activation and W_0 is the weight of the raw

110 materials before activation.

111 **2.3 Experimental design and response surface methodology**

112   RSM was applied to optimize the activation process as it is a useful statistical tool for

113 modeling and analysis of multivariable. This method was chosen for fitting a quadratic

114 surface with the fewest number of experiments. In this step, BBD method was applied in three

115 levels in order to design the activation experiments. Table 1 shows the ranges and levels of the

116 experimental parameters: mass ratio (X_1), activation time (X_2), and microwave power (X_3).

117 The MB adsorption (Y_1) was taken as the process responses.

118   In order to study the relationship between the response variable (MB number and yield) and

119 independent variables, the experimental data were fitted to a second-order polynomial

120 regression model, expressed by Eq. (2)

121 $$Y = \beta_0 + \sum_{i=1}^{k} \beta_i \chi_i + \sum_{i=1}^{k} \beta_{ii} \chi_i^2 + \sum_{i=1}^{k} \sum_{j=i+1}^{k} \beta_{ij} \chi_i \chi_j + \varepsilon \qquad (2)$$

122 where Y is the response variable, x_i and x_j are the independent variables, $\beta_0, \beta_i, \beta_{ii}$ and β_{ij}

123 are the regression coefficients (β_0 is constant term, β_i is the linear effect term, β_{ii} is

124 quadratic effect term, β_{ij} is the interaction effect term).

125   Design Expert software (version 8.0.6, Stat-Ease Inc., Minneapolis, USA) was used to

126 elaborate the experimental design, evaluate the model, and estimate the subsequent regression,

127 variance, and response surface analysis.

128 **2.4 Characterization of ASAC**

129   Some physical properties, textural morphology and chemical properties of ASAC were

130 measured by renowned analytical techniques. The surface physical properties of the ASAC

131 were characterized with Quanta Chrome Instruments Quadrasorb SI, using N_2 adsorption

132 measurements at 77 K. The S_{BET} was calculated with the (Brunauer-Emmett-Teller) BET

133 equation. The nitrogen volume held at the highest relative pressure ($P/P_0 = 0.95$) was used to

134 calculate the total pore volume of the ASAC. The micropores surface area, volume, and

135 external surface area were obtained using the t-plot method.

136   SEM was also employed to study the textural structure of the raw material and the

137 adsorbent after the activation process. The morphology of AS and ASAC were characterized

138 by SEM (JEOL, JSM-6490LV, Japan) with a secondary electron beam and an acceleration

139 voltage of 3 kV. The samples were coated with gold to ensure that the particles have suitable

140 conductivity after drying overnight at 80 °C under vacuum.

141   Chemical characterization of surface functional groups was inspected by FTIR (Magna-IR

142 750, Nicolet) in the scanning range of 4000–400 cm^{-1}, 10 scans were taken at a resolution of

143 1 cm^{-1}. The samples were mixed with KBr powder and the mixtures were pressed into pellet.

144   Meanwhile, the surface chemical element content at the surface of AS and ASAC was

145 performed using XPS. The XPS analysis was conducted using AMICUS/ESCA 3400

146 spectrometer with Mg radiation at 240 W and 12 kV under ultrahigh vacuum. Pass energy was

147 set as 276 and 300 eV for survey and high-resolution spectra, respectively. The XPS spectra

148 were calibrated by taking the graphitic peak as 284.5 eV. The surface atomic concentrations

149 were calculated from the survey spectra after correcting the relative peak areas by sensitivity

150 factors.

151   The determination of point of zero charge (pH$_{pzc}$) was conducted by adjusting the pH of 50

152 mL 0.1 mol/L NaCl solution (prepared in boiled water to eliminate CO_2) to a value between 2

153 and 12. Approximately 0.15 g of ASAC was added and the final pH was measured after 48 h

154 under agitation. The pH$_{pzc}$ is the point where pH$_{initial}$ − pH$_{final}$ = 0.

155 **2.5 Adsorption capacity**

156   0.1 g of ASAC was put into 150 mL Erlenmeyer flask with stopper containing 50 mL of

157 MB solution of initial concentration of 1.5 g/L at pH=6.16 for determining the adsorption

158 capacity of ASAC for MB. The flask was vibrated at 170 rpm in a thermostated waterbath

159 shaker at around 20 °C. After adsorption equilibrium time of 30 min, which obtained by a

160 series of preliminary experiments, Samples were separated by filtration, the concentration of

161 MB solution was analyzed by absorbance measurements using a double beam UV-75N at a

162 wavelength of 665 nm. The MB uptake of ASAC, q (mg/g), was calculated by Eq. (3):

163 $$q = \frac{(C_0 - C_e)V}{M} \tag{3}$$

164 where C_0 (mg/L) and C_e (mg/L) are the initial and equilibrium concentrations of MB,

165 respectively, V (L) is the volume of solution and M (g) is the dry mass of ASAC.

166 **2.6 Adsorption kinetics**

167   The procedures of the adsorption kinetics were carried out at the initial MB concentrations

168 set as 300 and 500 mg/L at 20 °C, respectively. 0.1g ASAC were put into 150 mL conical

169 flasks with 50 mL MB solution, the samples were separated by filtering at different contacting

170 time intervals (2, 5, 10, 15, 30, 45, 60, 120 min). And the residual concentrations of MB were

171 measured and adsorption amounts of ASAC were calculated with above method.

172   To understand the adsorption dynamics of MB on ASAC in relation to time, the

173 experimental data were analyzed using the pseudo-first-order [14] and pseudo-second-order

174 [15] kinetic models. The expression of the pseudo-first-order kinetic model is given by Eq.

175 (4):

176 $q_t = q_e(1-e^{-k1t})$ $\qquad\qquad\qquad\qquad\qquad\qquad\qquad\qquad\qquad$ (4)

177 where q_e (mg/g) is the amount of MB adsorbed at equilibrium, k_1 (h^{-1}) is the

178 pseudo-first-order rate constant, and t (h) is the contact time. The form of the

179 pseudo-second-order kinetic model is given by Eq. (5):

180 $$q_t = \frac{q_e^2 k_2 t}{1 + q_e k_2 t}$$ $\qquad\qquad\qquad$ (5)

181 where k_2 is the pseudo-second-order rate constant (g/mg min).

182 **2.7 Adsorption isotherms**

183   To analyze the validity of the adsorption data, the Langmuir and Freundlich adsorption

184 models were run as discussed below. Adsorption isotherms of activated carbon was

185 determined the adsorption amounts of different concentration (50, 200, 300, 550, 850, 910

186 and 1000 mg/L) of MB under the equilibrium adsorption time of 30 min.

187   The Langmuir isotherm equation [16], which is the most commonly used for monolayer

188   adsorption on to a surface with a finite number of identical sites, was represented by the

189   following Eq. (6):

190    $$q_e = \frac{q_m K_L C_e}{1 + K_L C_e} \qquad (6)$$

191   where C_e (mg/L) is the equilibrium concentration of the MB dye, q_m (mg/g) is the maximum

192   adsorption capacity and K_L (L/mg) is the Langmuir adsorption equilibrium constant (L/mg),

193   which is related to the affinity of the binding sites.

194   The Freundlich isotherm equation [17], the most important multilayer adsorption isotherm

195   for heterogeneous surfaces, is described by the following Eq. (7):

196    $$q_e = K_F C_e^{1/n} \qquad (7)$$

197   where K_F $((mg/g) \cdot (L/mg)^{-1/n})$ and n are Freundlich parameters related to the adsorption

198   capacity and adsorption intensity, respectively.

199   **3. Results and discussion**

200   **3.1. RSM and model fit**

201   BBD was used to elaborate correlation between the activated carbon preparation variables

202   to the MB adsorption and yield. Seventeen experiments were performed for the RSM

203   optimization of three parameters at three levels. The results of these experiments are

204   presented in Table 1. Runs 13–17 at the center point were used to check the experimental error.

205   The Q_m values for ASACs, which were prepared according to the experimental conditions,

206   ranged from 164.82 to 314.20 mg/g, while the yield of carbon obtained ranged from 31.0% to

207   49.7%. For the response of MB adsorption value, the quadratic model was selected, as

208   suggested by the software. The final empirical model in terms of coded factors for MB

209   adsorption value (Y_1) was shown in Eq. (8)

210    $Y_1 = 203.71 + 44.81X_1 + 7.46X_2 + 18.67X_3 + 3.70X_1X_2 + 11.17X_1X_3 - 11.24X_2X_3 + 23.45X_1^2$

211    $- 13.79X_2^2 + 1.17X_3^2$ (8)

212   Negative signs in front of the terms indicate antagonistic effects, whereas the positive signs

213   indicate synergistic effects. Variance was employed to justify the adequacy of the model.

214   Variance for the quadratic model of MB adsorption is shown in Table 2, where the F-value of

215   9.92 and Pr > F of 0.0032 proved that the model is significant. The value of model terms Pr >

216   F less than 0.05 indicates that the model terms are significant. The results showed that X_1, X_3

217   and X_1^2 are all significant model terms. These significant effects signified the importance and

218   effectiveness of the selected independent variables for the experiments. As shown in the

219   variance analysis, the lack-of-fit-test was non-significant, indicating that the model can be

220   well fitted to the studied data. The 3D response surface (Fig. 1) is generally the graphical

221   representation of the regression equation. The effect of heating time on the experimental

222   response of Q_m values can be seen in Figs. 1a and 1c. The heating time has only a weak effect

223   on the MB adsorption capacity. The indistinctive effect of the microwave heating time on the

224   adsorption capacity values was also reported by Zhong et al. [18]. Fig. 1a and 1b exhibited the

225   effect of the mass ratio on the response. The value of Q_m evidently increased with the increase

226   in mass ratio at high microwave power levels. The use of the activating reagent in the

227   microwave-assisted activation could promote the breaking of bonds in the precursors and

228   elimination of some volatile species from the precursors [19]. As a result, ASACs with

229   increased surface area and higher adsorption capacity are obtained. Our results on the effect of

230   microwave power (Figs. 1b and 1c) demonstrated that the highest values of Q_m could be

231 obtained at a microwave powers over 820 W. This trend was attributed that the high

232 microwave power could increase the temperature of the system, reduce the activation energy

233 of the carbon–reagent reaction and promote the development of pores on the materials [20].

234 **Fig. 1 should be put here.**

235 **3.2 Process optimization**

236   The preparation of ASAC with adsorption efficiency toward organic compounds, such as

237 MB dye, is the most important aspect of its potential economic feasibility and marketing.

238 Design Expert software version 8.0.6 was used to compromise adsorption capacity while

239 optimizing the value by selecting the highest responses from the experimental results. The

240 optimum calculated conditions were a mass ratio of 3:1, an activation time of 15 min, and a

241 microwave power of 900 W. Under optimal conditions, a carbon yield of 41.19% and an MB

242 adsorption capacity of 285.69 mg/g were predicted. Meanwhile, the practical repeat

243 experiments were carried out to justify the accuracy of the predicted results which showed the

244 carbon yield of 39.67% and an MB adsorption capacity of 314.20 mg/g. The relative errors

245 for the carbon yield and MB adsorption capacity between the experimental and predicted

246 values are 3.69% and 9.07%, respectively, which indicates the sufficient accuracy of the

247 process optimization. The present study reveals the remarkable adsorption capacity of MB

248 onto ASAC (Table 3) as compared to previously reported adsorbents [11, 21-23].

249 **3.3 Characterization of ASAC**

250 **3.3.1 Specific surface area and pore structure of ASAC**

251   The N_2 adsorption–desorption isotherm at 77 K is shown in Fig. 2a. The isotherm

252 resembles a combination of type I and type II isotherms, as defined by IUPAC; this adsorption

253 behavior exhibits characteristics of microporous–mesoporous structures [24]. The pore size

254 distribution of ASAC is shown in Fig. 2b. The sharpest peak is observed at a pore diameter

255 between 0.5 and 1.0 nm, with an average pore size of 0.83 nm, which indicated the essentially

256 microporous texture of ASAC. The specific surface area was calculated by the BET equation,

257 which was 839.60 m^2/g. The structural characteristics of ASAC are listed in Table 4. ASAC

258 exhibited a relatively high S_{BET} of 839.60 m^2/g and a V_T of 0.406 cm^3/g as compared to

259 previous studies.

260 **Fig. 2 should be put here.**

261 **3.3.2 SEM analysis of ASAC**

262 Fig. 3 shows SEM images of AS and ASAC prepared under the optimum conditions (i.e.,

263 mass ratio of 3:1, activation time of 15 min, and microwave power of 900 W). The surface of

264 the AS is planar, undulating and mainly consists of macropores. The number of pores of the

265 ASAC significantly increased after the activation process. ASAC surface exhibited a

266 well-organized, pronounced, and uniform porosity (Fig. 3b), which significantly increased its

267 surface area, and resulted in more pores available for MB adsorption. This observation was

268 supported by the physical parameters as summarized in Table 3, which highlighted the pore

269 development during the microwave irradiation period. A similar phenomenon was also

270 observed by Njoku et al., who reported the surface morphology of rambutan peel-based ACs

271 having a series of uniform cavities around the surface due to activation by KOH [4].

272 **Fig. 3 should be put here.**

273 **3.3.3 Functional groups analysis of ASAC**

274 The surface chemistry of AS and ASAC was studied by FTIR spectroscopy in the infrared

275   spectral region of 4000–400 cm^{-1} (Fig. 4). AS contained much more bands than ASAC, with

276   some major differences. The broad band at approximately 3450 cm^{-1} was observed for all

277   samples, which was attributed to the O–H stretching vibration of the hydroxyl functional

278   groups [13, 27]. The intense band at approximately 2950 cm^{-1} for AS was assigned to the

279   C–H stretching vibration [28], which disappeared for ASAC, indicating the removal of

280   hydrogen by activation. A band at approximately 2359 cm^{-1} for AS and ASAC was attributed

281   to C≡C (alkynes), which was also reported similarly by Foo et al. [29]. A series of complex

282   bands was detected in the range of 800–1630 cm^{-1} for AS, which was significantly reduced

283   after activation. This phenomenon is possibly due to the breakdown of the chemical bonds in

284   the raw material [30]. Compared with the bands located at 1630, 1390, 1255, 1085 and 800 in

285   the spectra of the AS attributed to O-H bending vibrations, C-O-C (esters or phenol), C-O-C

286   (ether) group, C-O stretching vibration and C-H blending or benzene, these bands in ASAC

287   were weakened [5, 31]. The signal at 550 cm^{-1} was assigned to the C–O–H bending vibration

288   [32].

289   **Fig. 4 should be put here.**

290   The compositional chemistry of surfaces of both AS and ASAC was analyzed by XPS, as

291   shown in Fig. 5a. The observed spectra contained distinct peaks for C and O. The relative

292   content of these elements was calculated and listed in Table 5. The percentage amounts of C,

293   O, and S were: 72.07%, 26.88%, and 1.05% in AS and 86.57%, 13.43% and 0.00% in ASAC,

294   respectively, thereby indicating a small increase in the C amount and a decrease in the O

295   amount after activation procedure.

296   The high-resolution spectra of C 1s and O 1s were further analyzed by a curve-fitting

297 procedure, based on the Gaussian–Lorentzian function after baseline subtraction with

298 Shirley's method. Four components were considered to comprise the C 1s spectra [33] with

299 chemical shifts corresponding to: C–C (284.5 eV), C–O–R (285.8 eV), C=O (287.0 eV), and

300 COOR (289.2 eV). The fitting curves of these groups are illustrated in Fig. 5b-c, Fig. 5d-e

301 shows the deconvolution of the O 1s spectra for the AS and ASAC produced four peaks at

302 533.3, 534.2, 535.1, and 535.7 eV; these peaks represented O=C, O-C, R-O-C=O, and

303 C-OOH, respectively, and the relative content of each group is listed in Table 5. The results

304 suggest that the C–C group was predominant for the ASAC, which comprised close to 60% of

305 the carbon species. Moreover, relative contents of oxygen showed a significant decrease. For

306 oxygen species, the analysis suggested an increase in C=O group and a decrease in other

307 oxygen-groups for the ASAC (Fig. 5d-e). Liu et al. showed a similar phenomenon with the

308 reduction of oxygen-containing groups in AC, which is consistent with the FTIR and XPS

309 spectra [34].

310 **Fig. 5 should be put here.**

311 **3.4 Adsorption studies of MB**

312 **3.4.1 Effect of pH on the adsorption of MB onto ASAC**

313 The adsorption behavior of MB onto ASAC at different pH values was shown in Fig. 6.

314 The effect of pH was conducted by varying the pH of dye solutions from 2 to 12 with an

315 initial concentration of 500 mg/L, and the adsorption capacity showed an increase with the

316 increase of pH. Particularly, the adsorption capacity has a significant enhancement at pH of

317 6-8, which could be related to the protonation of MB in acidic medium, which triggers a

318 competitional effect between excessive amounts of H^+ and cationic dye on adsorption sites.

319 As the solution pH increases, ASAC may become more negatively charged and the formation

320 of such electric double layer facilitates in changing the polarity, which lead into the

321 enhancement of adsorption capacity. The effect of pH can be described on the basis of pH_{pzc}.

322 The pH_{pzc} of ASAC was identified to be 6.16. When the solution $pH < pH_{pzc}$, activated carbon

323 adsorbent will react as a positive surface, but when the solution $pH > pH_{pzc}$, it will act as a

324 negative surface. Therefore, for pH values above 6.16, the formation of electric double layer

325 changes its polarity, which causes an increase in the surface charge density and electrostatic

326 force of attraction. It unveils the dual adsorption of MB onto ASAC i.e. Physical adsorption as

327 well as chemical adsorption, and the mechanism of chemical adsorption include the reaction

328 between hydroxyl and carbonyl functional groups on the surface of the ASAC and MB.

329 Positive charge on MB and OH^- on ASAC react according to the following reaction:

330

$$(9).$$
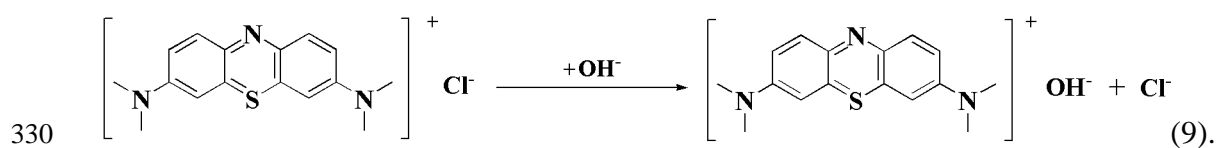
331 **Fig. 6 should be put here.**

332 **3.4.2 Adsorption kinetics**

333 The experimental data obtained for the AC from the initial concentrations of MB solution

334 (300 and 500 mg/L) were fitted to the pseudo-first-order and pseudo-second-order models

335 (Fig. 7). Rapid adsorption occurred in the first 15 minutes and reached the equilibrium after

336 30 min, which indicates the favorable interaction between the adsorbent and adsorbate (Table

337 6). The data indicate that the adsorption of MB onto ASAC was best described by the

338 pseudo-second-order model, which $R^2 = 0.999$, similar values of q_e were calculated and

339 experimentally determined. These findings suggest that the MB–ASAC system followed the

340   pseudo-second-order model, and the overall rate of adsorption process was controlled by

341   physisorption at the beginning of adsorption and chemisorption after the first stage, which has

342   already been explained by the effect of pH on the adsorption of MB onto ASAC. The same

343   behavior was also observed by Foo et al. [29].

344   **Fig. 7 should be put here.**

345   **3.4.3 Adsorption isotherms**

346   The plots of the nonlinear Langmuir and Freundlich isotherm models for the adsorption of

347   MB onto ASAC at 20 °C in line with Eq. (6) and (7) are presented in Fig. 8. The isotherm

348   parameters determined from the slopes, as well as with the correlation coefficients of the

349   isotherm models are summarized in Table 7. The equilibrium data were valid for the

350   Langmuir isotherm model ($R_{adj}^2 = 0.989$), demonstrating the adsorption of MB onto ASAC

351   from aqueous solutions by a monolayer formation. This result was in conformity with the

352   previous result of nitrogen adsorption-desorption authenticating the monolayer adsorption

353   phenomenon. The present results are quite consistent with previous researches on the

354   adsorption of MB onto ACs prepared from pomelo skin and oil palm (*Elaeis*) empty fruit

355   bunch by microwave-assisted chemical activation [32, 35].

356   **Fig. 8 should be put here.**

357   **4. Conclusions**

358   This study proposes a remarkable adsorbent ASAC through microwave heating method

359   from the agricultural waste of AS. RSM was successfully used to optimize the conditions for

360   ASAC preparation. The optimal activation conditions are as follows: a mass ratio ($ZnCl_2$/AS)

361   of 3:1 (w/w), a microwave heating time of 15 min, and a microwave power of 900 W. The

362 resulting BET surface area of ASAC was 839.60 m^2/g, and the total pore volume was 0.406

363 cm^3/g. The yield and MB adsorption of ASAC under optimum conditions were 39.67% and

364 314.20 mg/g, respectively. These results indicated that the mass ratio and microwave power

365 were the significant factors that affected carbon yield and MB adsorption. All statistical tools

366 proved the excellent operational efficiency of ASAC. The adsorption behavior could be

367 favorably described by the pseudo-second-order models and Langmuir isotherm. The

368 excellent adsorption capacity of ASAC against MB validated its supremacy over the so far

369 reported absorbents. Thus, the short microwave heating time and simplicity of the process

370 demonstrated that microwave-assisted activation is a promising method for converting the AS

371 into an excellent adsorbent, which could be employed in the remediation of aquatic

372 environment as well as in chemical industry.

Acknowledgments

377

References

378

[1] Walker GM, Weatherley LR. Sep. Sci. Technol. 2000, 35, 29-1341.

[2] Hesas RH, Arami-Niya A, Daud WMAW, Sahu JN. Chem. Eng. Res. Des. 2013, 91, 2447-2456.

[3] Tan IAW, Ahmad AL, Hameed BH. Chem. Eng. J. 2008, 137, 462-470.

[4] Njoku VO, Foo KY, Asif M, Hameed BH. Chem. Eng. J. 2014, 250, 198-204.

[5] Xiao H, Peng H, Deng SH, Yang XY, Zhang YZ, Li YW. Bioresour. Technol. 2012, 111, 127-133.

[6] Saka C. J. Anal. Appl. Pyrol. 2012, 95, 21-24.

[7] Wang X, Liang X, Wang Y, Wang X, Liu M, Yin D, Xia S, Zhao J, Zhang Y. Desalination 2011, 278, 231-237.

[8] Achawa OW and Afraneb G. Micropor. Mesopor. Mat. 2008, 112, 284-290.

[9] Ozhan A, Sahin O, Saka C, Kucuk MM. Cellulose. 2014, 21, 2457-2467

[10]J. Pezoti junior O, Cazetta AL, Gomes RC, Barizao EO, Souza IPAF, Martins AC, Asefa T, Almeida VC. Anal. App. Pyrol. 2014, 105, 166-176.

[11]Xiao XM, Tian F, Yan YJ, Wu ZS. J. Shihezi Univ. 2014, 4, 485-490.

[12]Xiao XM, Tian F, Yan YJ, Wu ZS, Wu ZL, Cravotto G. Korean J. Chem. Eng. 2015, 32, 1129-1136..

[13]Sahu JN, Acharya J, Meikap BC. Bioresour. Technol. 2010, 101, 1974-1982.

[14]Guses A, Dogar C, Yalcin M, Acikyildiz M, Bayrak R, Karaca S. J. Hazard. Mater. 2006, 131, 217-228.

[15]Al-Ghouti MA, Khraisheh MAM, Ahmad MNM, Allen S. J. Hazard. Mater. 2009, 165,

400   589-598.

401   [16]Ge XY, Tian F, Wu ZL, Yan YJ, Cravotto G, Wu ZS. Chem. Eng. Process. 2015, 91,

402   67-77.

403   [17]Freundlich H. Z. Phys. Chem. 1906, 57, 384-470.

404   [18]Zhong ZY, Yang Q, Li XM, Luo K, Liu Y, Zeng GM. Ind. Crop. Prod. 2012, 37, 178-185.

405   [19]Basta AH, Fierro V, El-Saied H, Celzard A. Bioresour. Technol. 2009, 100, 3941-3947.

406   [20]Duan XH, Srinivasakannan C, Peng JH, Zhang LB, Zhang ZY. Fuel Process Technol.

407   2011, 92, 394-400.

408   [21]Brum SS, Bianch ML, Silva VL, Goncalves M, Guerreiro MC, Oliveira LCA. Quim.

409   Nova 2008, 31, 1048-1052.

410   [22]Deng H, Yang L, Tao GH, Dai JL. J. Hazard. Mater. 2009, 166, 1514-152.

411   [23]Foo KY, Hameed BH. Bioresour. Technol. 2012, 111, 425-432.

412   [24]Kruk M, Jaroniec M. Chem. Mater. 2001, 13, 3169-3183.

413   [25]Foo KY, Hameed BH. Biomass Bioenerg. 2011, 35, 3257-3261.

414   [26]Foo KY, Hameed BH. Bioresour. Technol. 2011, 102, 9814-9817.

415   [27]Ge XY, Ma XF, Wu ZS, Xiao XM, Yan YJ. Res. Chem. Intermediat. 2015, 41,

416   7327-7347.

417   [28]Foo KY, Lee LK, Hameed BH. Chem. Eng. J. 2013, 223, 604-610.

418   [29]Foo KY, Hameed BH. Chem. Eng. J. 2012, 180, 66-74.

419   [30]Yagmur E. J. Porous Mat. 2012, 19, 995-1002.

420   [31]Silverstein, RM, Webster, FX, Kiemle, DJ, Spectrometric Identification of Organic

421   Compounds, 7th ed., John Wiley and Sons, New York, 2006.

422   [32]Foo KY, Hameed BH. Chem. Eng. J. 2011, 173, 385-390.

423   [33]Ryu Z, Rong H, Zheng J, Wang M, Zhang B. Carbon 2002, 40, 1131-1150.

424   [34]Liu QS, Zheng T, Wang P, Guo L. Ind. Crops Prod. 2010, 31, 233-238.

425   [35]Foo KY, Hameed BH. Desalination 2011, 275, 302-305.

426

Table captions

Table 1 Factorial design matrix and experimental response values.

Table 2 Analysis of variance for response surface quadratic model for adsorption capacity of MB.

Table 3 Comparison of adsorption capacities of various adsorbents for MB.

Table 4 Surface physical characteristics of the ASAC and other ACs.

Table 5 Relative contents of various elements and peak parameters of different C $1s$ and O $1s$ components of AS and ASAC samples based on the XPS spectra.

Table 6 Pseudo-first-order and pseudo-second-order kinetic rate constants for the adsorption of MB onto ASAC at 20 °C.

Table 7 Isotherm model parameters for the adsorption of MB onto ASAC at 20 °C.

439 **Table 1**

Std	Run	Mass ratio X_1(w/w)	Microwave heating time X_2(min)	Microwave power X_3(W)	Y_1(mg/g)	Y_2 (%)
3	1	1:1	20	700	179.80	36.00
11	2	2:1	10	900	209.81	34.70
1	3	1:1	10	700	164.83	35.50
7	4	1:1	15	900	194.73	37.00
6	5	3:1	15	500	239.59	40.00
12	6	2:1	20	900	194.81	36.00
8	7	3:1	15	900	314.20	39.67
2	8	3:1	10	700	239.55	34.00
5	9	1:1	15	500	164.82	38.50
10	10	2:1	20	500	194.86	31.00
4	11	3:1	20	700	269.32	39.00
9	12	2:1	10	500	164.92	49.70
16	13	2:1	15	700	224.64	38.70
13	14	2:1	15	700	209.56	42.00
14	15	2:1	15	700	179.79	45.00
17	16	2:1	15	700	194.74	38.70
15	17	2:1	15	700	209.83	63.30

440

441 **Table 2**

Source	Sum of squares	DF	Mean square	F-Value	Prob. > F
Model	23349.22	9	2594.36	9.92	0.0032
X_1	16063.49	1	16063.49	61.41	0.0001
X_2	445.21	1	445.21	1.70	0.2333
X_3	2788.55	1	2788.55	10.66	0.0138
X_1X_2	54.76	1	54.76	0.21	0.6611
X_1X_3	499.52	1	499.52	1.91	0.2095
X_2X_3	504.90	1	504.90	1.93	0.2073
X_1^2	2315.18	1	2315.18	8.85	0.0207
X_2^2	800.23	1	800.23	3.06	0.1238
X_3^2	5.80	1	5.80	0.022	0.8858
Residual	1831.09	7	261.58		
Lack of fit	668.72	3	222.91	0.77	0.562
Pure error	1162.37	4	290.59		
Cor total	25180.31	16			

442

443

Table 3

Precursors of ACs	Mass of AC (g)	Initial concentrations of MB (mg/L)	Volume of MB (mL)	pH	Adsorption capacity of MB (mg/g)	References
Macadamia nut endocarp	0.025	500	25	-	194.7	[11]
Coffee waste	0.1	1000	10	5.3	188.7	[22]
Cotton stalk	0.1	1500	25	-	193.5	[23]
Wood sawdust	0.2	500	200	-	425.3	[24]
Almond shell	0.1	1500	50	6.16	314.2	This work

445

446

Table 4

Precursors of ACs	S_{BET} (m^2/g)	Micropore area (m^2/g)	V_T (cm^3/g)	Micropore Volume (cm^3/g)	Average pore width (nm)	References
Almond shell	839.60	383.64	0.406	0.152	0.83	This work
Pistachio shell	700.53	-	0.375	-	2.14	[25]
Rice husk	752	346	0.64	0.26	3.41	[26]
Cotton stalk	794.84	156.69	0.63	0.083	3.20	[23]

448

449

450

451 **Table 5**

	Relative content (%)			Relative content (%) of C 1s				Relative content (%) of O 1s			
	C	O	S	C-C	C-O-R	C=O	C-OOR	C=O	C-O	C-OOR	C-OOH
AS	72.07	26.88	1.0	13.15	41.97	25.59	19.29	22.55	32.73	24.05	20.67
ASAC	86.57	13.43	0.0	59.18	22.18	11.47	7.17	39.17	26.21	17.18	17.44

452

453

454

455 **Table 6**

C_0(mg/L)	$q_{e,exp}$(mg/g)	Pseudo-first-order			Pseudo-second-order		
		K_1(mg/g)	q_e(mg/g)	R^2	K_2(g/mg)	q_e(mg/g)	R^2
300	148.59	0.770	148.45	0.785	0.050	149.25	0.999
500	249.56	0.508	248.51	0.842	0.160	250.00	0.999

456

457

458

459 **Table 7**

Isotherms	Langmuir			Freundlich		
Constants	q_m (mg/g)	K_L (L/mg)	R^2	n	K_F (mg/g)(L/mg)$^{1/n}$	R^2
	500.00	0.307	0.989	2.22	112.449	0.717

460

461

462

Figure captions
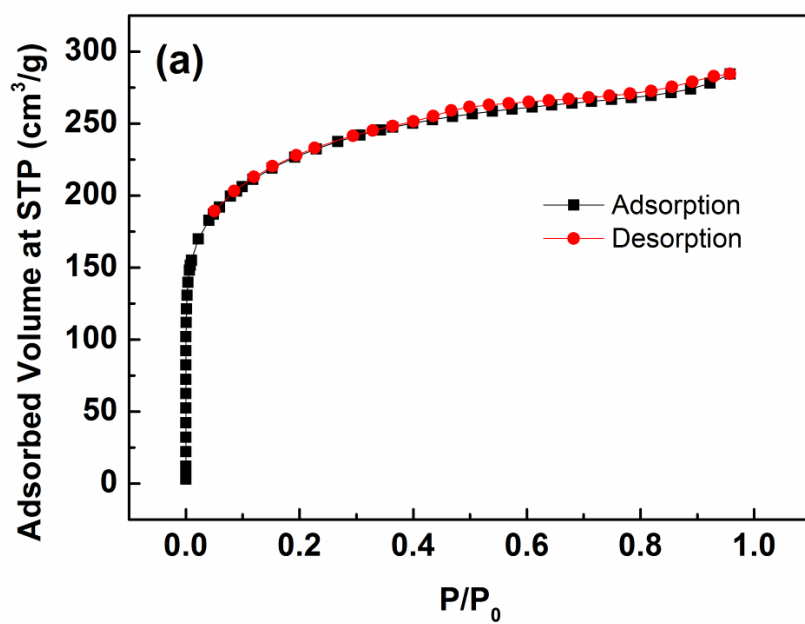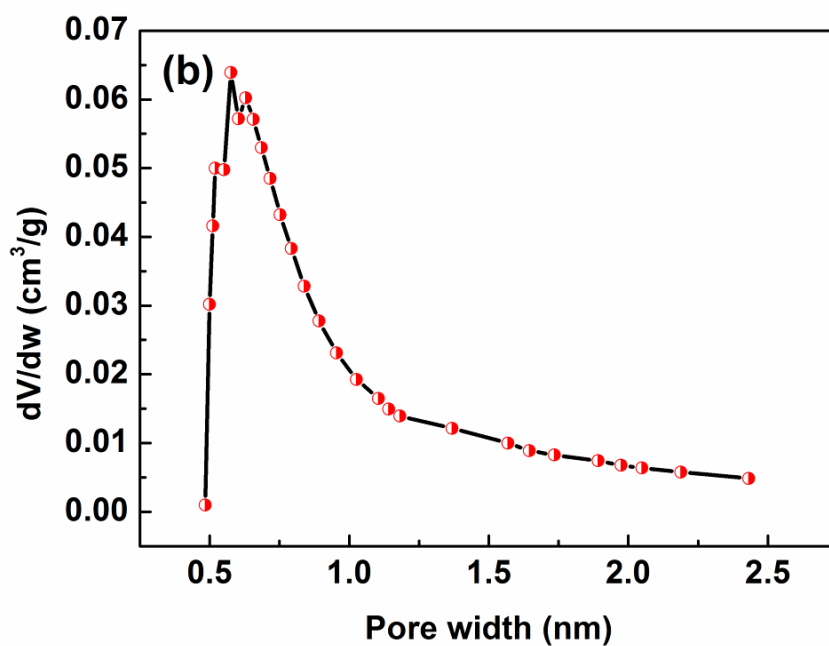
Fig. 1 Three-dimensional graphic of response surface for response: mass ratio and activation time (a), mass ratio and microwave power (b), activation time and microwave power (c).

Fig. 2 N_2 adsorption and desorption isotherms at 77K (a) and pore size distribution (b) of ASAC.

Fig. 3 SEM images of AS (a), and ASAC (b).
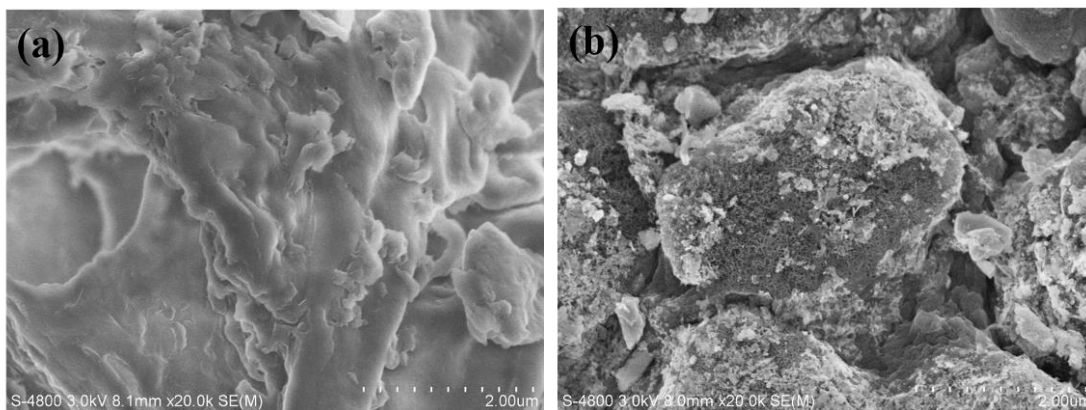
Fig. 4 FTIR spectra of AS and ASAC.

Fig. 5 XPS survey spectra and high-resolution spectra of AS and ASAC: (a) survey scans; (b) AS: C 1s; (c) ASAC: C 1s; (d) AS: O 1s; (e) ASAC: O 1s.

Fig. 6 Effect of pH on the adsorption of MB onto ASAC at 20 °C (C_0 = 500 mg/L, contact time = 30 min, activated carbon mass = 0.1 g)

Fig. 7 Effect of time on the adsorption of MB onto ASAC at 20 °C (pH = 6.16, 0.1 g of ASAC).

Fig. 8 Plots of Langmuir and Freundlich models for adsorption of MB onto ASAC (pH = 6.16, contact time = 30 min, 0.1 g of ASAC).

485

486

487

Fig. 1 Three-dimensional graphic of response surface for response: mass ratio and activation time (a), mass ratio and microwave power (b), activation time and microwave power (c).

490

491

492

Fig. 2 N$_2$ adsorption and desorption isotherms at 77K (a) and pore size distribution (b) of
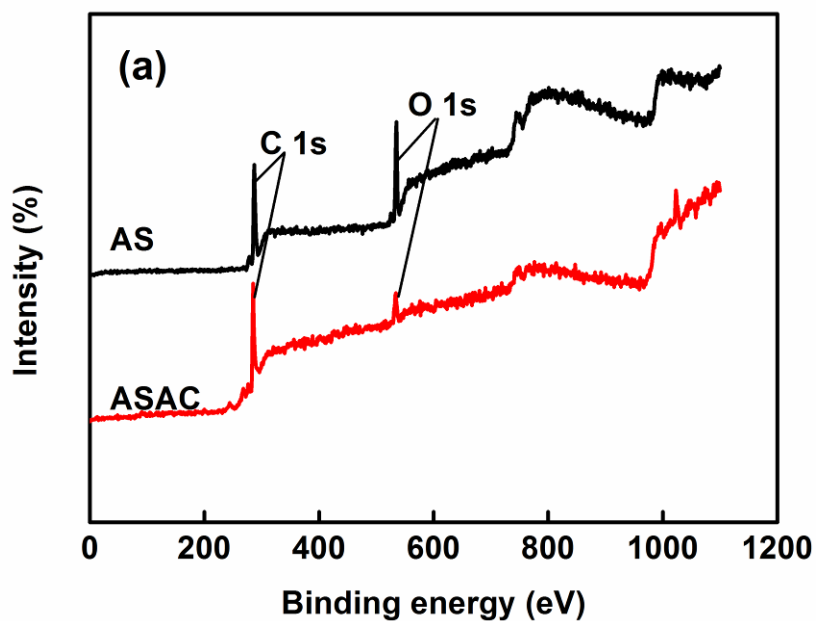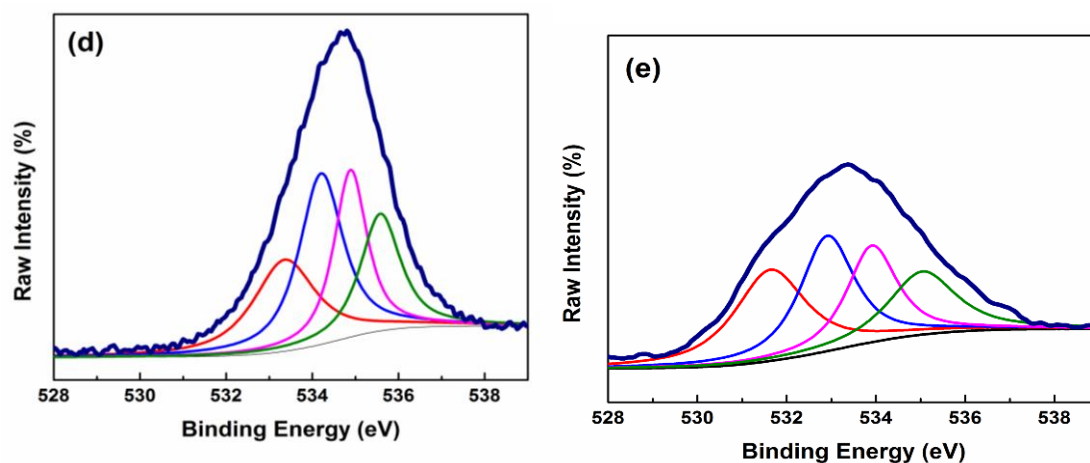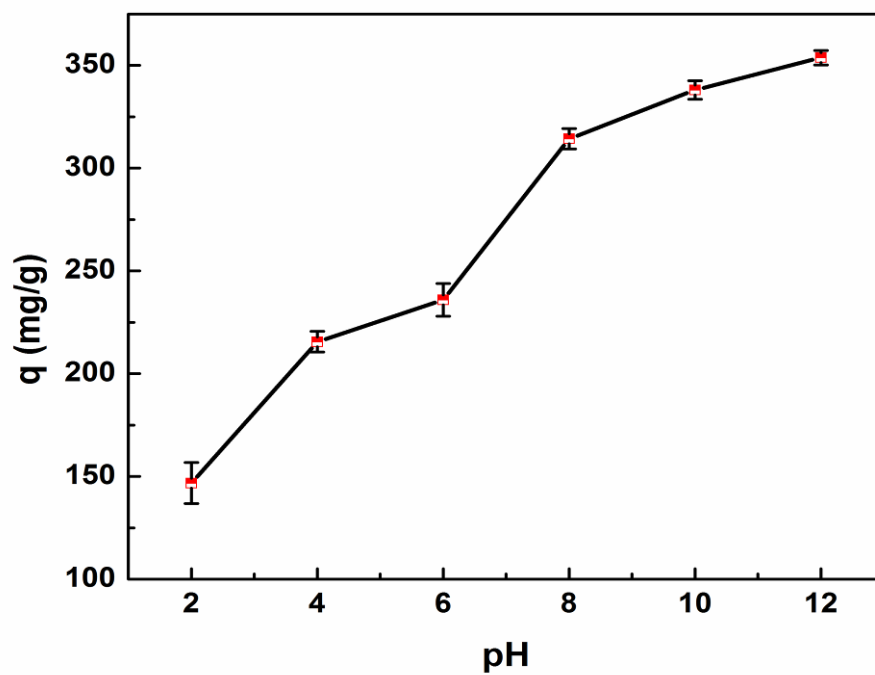ASAC.

495

496

497

498

499

500

501
502

503

Fig. 3 SEM images of AS (a), and ASAC (b).

505
506
507
508

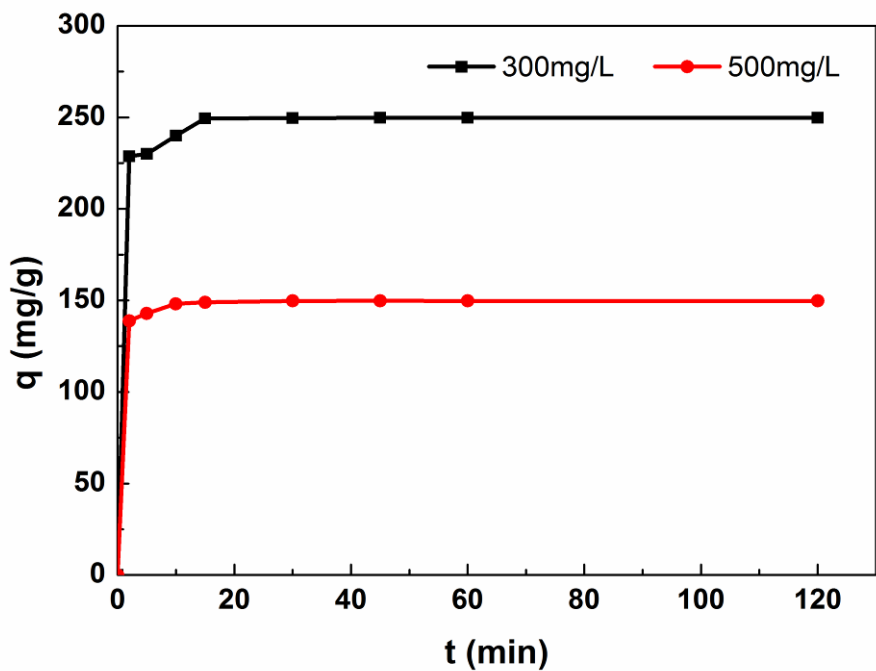509

Fig. 4 FTIR spectra of AS and ASAC.

511
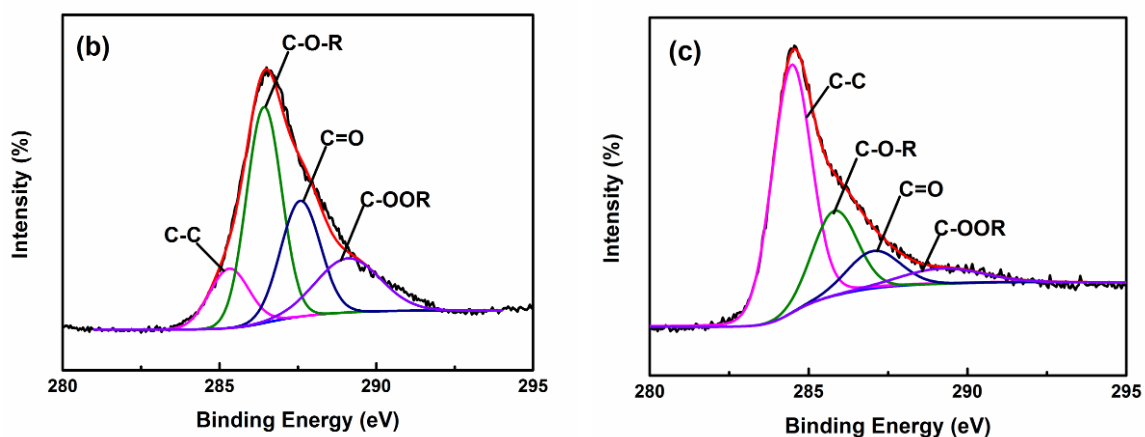
512

513

Fig. 5 XPS survey spectra and high-resolution spectra of AS and ASAC: (a) survey scans; (b)

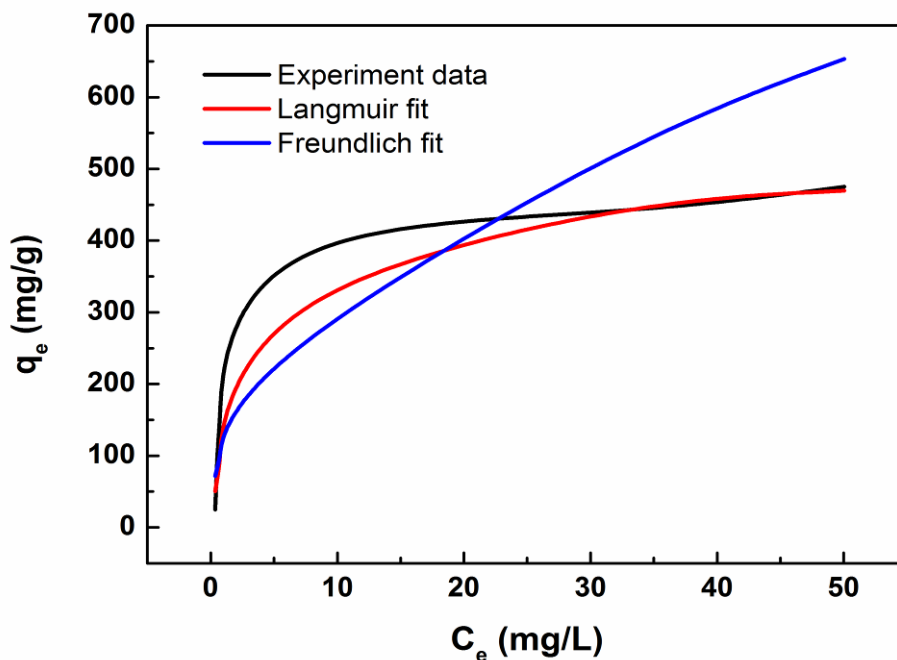AS: C 1*s*; (c) ASAC: C 1*s*; (d) AS: O 1*s*; (e) ASAC: O 1*s*.

516
517

518

519 **Fig. 6** Effect of pH on the adsorption of MB onto ASAC at 20 °C (C_0 = 500 mg/L, contact

520 time = 30 min, activated carbon mass = 0.1 g)

521

522

Fig. 7 Effect of time on the adsorption of MB onto ASAC at 20 °C (pH = 6.16, 0.1 g of

524   ASAC).
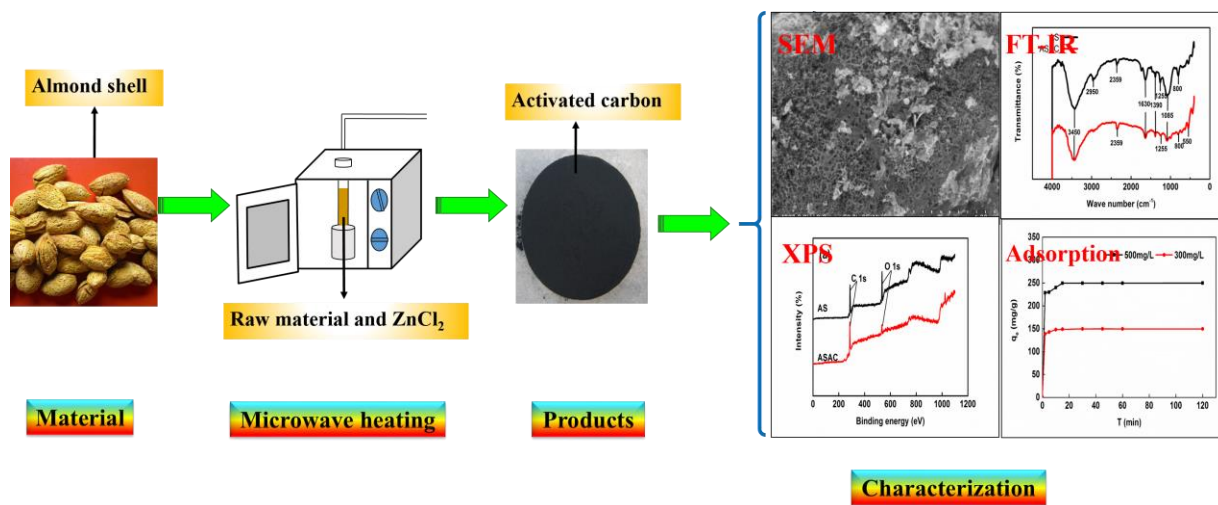

525

526   **Fig. 8** Plots of Langmuir and Freundlich models for adsorption of MB onto ASAC (pH = 6.16,

527   contact time = 30 min, 0.1 g of ASAC).

528   **Graphical abstract figure**

529